

# Populating and probing protected edge states through topology-entailed trivial states

Francesco S. Piccioli,<sup>1,2</sup> Mark Kremer,<sup>1</sup> Max Ehrhardt<sup>1</sup>, Lukas J. Maczewsky<sup>1</sup>, Nora Schmitt<sup>3</sup>, Matthias Heinrich<sup>1</sup>, Iacopo Carusotto<sup>2</sup>, Alexander Szameit<sup>1\*</sup>

<sup>1</sup>Institute for Physics, University of Rostock,  
Albert-Einstein-Str. 23, 18059 Rostock, Germany

<sup>2</sup>University of Trento and CNR-INO BEC center,  
Via Sommarive 14, 38123 Povo (TN), Italy

<sup>3</sup>Institut für Experimentalphysik, Universität Hamburg  
Luruper Chaussee 149, 22761 Hamburg, Germany

\* corresponding author: alexander.szameit@uni-rostock.de

Topological insulators enable non-reciprocal light propagation that is insensitive to disorder and imperfections. Yet, despite considerable attention from the photonics community and beyond, the very feature that has inspired numerous proposals for applications of topological transport also turns out to be one of the main stumbling blocks for practical implementations: Accessing topologically protected states is generally assumed to require their protection to be lifted. We overcome this limitation by topology-entailed trivial (TET) states that arise from the hybridization of counter-propagating interface states. We demonstrate selective injection and extraction of light into topological states as well as long-range coherent light exchange between spatially separated topological channels. Our results highlight the potential of TET states as protection-preserving paradigm to manipulate the flow of light in topological platforms.

**One sentence Summary:** TET states allow local access to topological channels and long-range bidirectional links between distant protected states.

The topological origin of chiral edge states is at the root of their extreme robustness [1,2]. In the context of photonics [3–5], topological protection allows light encountering generic imperfections or defects to find its way around them without being subject to back reflections or scattering into the bulk, and while merely accumulating a phase shift [6–10]. Such channels generally exist along edges of the system (Fig. 1a) or an interface between two topologically distinct domains (Fig. 1b). In recent years, the implications of this new class of synthetic materials have been explored along many different directions, ranging from robust microwave devices to non-magnetic non-reciprocity and topological lasing [11–16]. Regardless of the specific context, populating a topological mode, having it interfere with other topological modes, or deliberately extracting energy from it are essential yet challenging tasks.

Currently, the perhaps most widespread strategy along these lines is based on out-of-plane injection [12] and/or extraction [8,12] from a higher dimension. While this approach is highly efficient for planar arrangements, is impractical in three- or higher-dimensional topological systems for obvious reasons. Another method employs evanescent coupling, where additional waveguides [8] or ancillary “straw” arrays [17] are placed in close proximity to gradually populate the topological mode. Yet, this mechanism likewise is subject to certain limitations: Crucially, the evanescent interaction between two guiding structures decays exponentially with their distance, requiring the injection structure to be placed in the immediate vicinity to facilitate meaningful transfer rates. Similarly, the energy scale associated with the coupling strength between the straw and the topological structure inherently limits the fidelity with which the desired mode can be excited in the presence of energetically similar bulk modes. More generally, the presence of a strongly-coupled external element will inevitably destroy topological protection.

As we will show in the following, TET states naturally serve to overcome these limitations by enabling selective local interactions with topological states. In this vein, they can readily facilitate both injection into and extraction from the topological channel without compromising its protection. TET states are bi-directional entities that arise due to the hybridization of two conventional counter-propagating topological states at the interface between two topologically identical domains that nevertheless are distinguishable by some other parameter (Fig. 1c). We illustrate these physics using a three-step anomalous Floquet driving protocol [18–20] in which the hopping between adjacent lattice sites is cyclically enabled in three distinct steps (Fig. 2a). Under these conditions, TET states can readily be established by introducing a detuned domain in which the on-site *quasi energy* systematically differs from that in the other domain. Moreover, we show that TET states, despite being strictly speaking topologically trivial, are fundamentally rooted in the topological properties of the host system and therefore inherit an unusual degree of robustness compared to conventional trivial states (c.f. Supplementary). As a result, TET states enable new strategies for manipulating the flow of light in complex all-topological photonic networks. They are of particular interest for, e.g., topological lasers [13,16], but more generally allow for the efficient interfacing between spatially sep-

arated conventional topological states in contexts where “every photon counts,” such as quantum-optical topological systems [21–24] or ultra-sensitive sensing applications.

## 1 Theoretical model

As well-known example of photonic topological structure, we base our study on an anomalous Floquet Insulator with honeycomb geometry, the so-called Kitagawa model [18]. As schematically illustrated in Fig. 2a, this model features a time-periodic tight-binding Hamiltonian, in which three piece-wise constant steps of duration  $T/3$  form one period  $T$  of the driving protocol. In each step, inter-site coupling of magnitude  $C$  is exclusively established between neighboring sites along one of the three lattice vectors, as represented by the  $\mathbf{k}$ -space Hamiltonian:

$$H(\mathbf{k}, t + T) = H(\mathbf{k}, t) = \sum_{i=1}^3 \mathbb{1}_{T_i}(t) \begin{pmatrix} 0 & Ce^{j\mathbf{k} \cdot \mathbf{b}_i} \\ Ce^{-j\mathbf{k} \cdot \mathbf{b}_i} & 0 \end{pmatrix}.$$

Here,  $\mathbb{1}_{T_i}(t)$  and  $\mathbf{b}_i$  are the indicator function and the respective coupling direction of the  $i$ -th time step. According to Floquet theory for time-periodic Hamiltonians, this introduces a  $2\pi/T$ -periodicity to the quasi-energies of the system. As a consequence, a *quasi-energy Brillouin zone* can be identified  $\epsilon \in [-\pi/T, \pi/T]$  here consisting in two non-degenerate bands and two bandgaps, one at the center (around  $\epsilon = 0$ , henceforth referred to as “0 gap”) and one at the edge of the quasi-energy Brillouin zone (at  $\epsilon = \pm\pi/T$ , accordingly termed “ $\pi$  gap”).

The topological properties of this system are described by the (2+1)D winding number  $\mathcal{W}$ , which can be calculated for different values of the so-called coupling phase  $\theta_c = C \cdot T/3$ . For  $\pi/3 < \theta_c < 2\pi/3$  the system is in the anomalous Floquet topological insulating (A-FTI) phase [18] characterized by  $\mathcal{W}_0 = \mathcal{W}_\pi = 1$ , where  $\mathcal{W}_\epsilon$  is the winding number at the quasi-energy  $\epsilon$ . Consequently, a finite lattice in the A-FTI phase supports chiral edge states crossing both the 0 and  $\pi$  gaps with the same chirality (Fig. 2b).

Let us now consider two adjacent domains adhering to same model and place them in contact with an inter-system coupling strength  $C_s$ . If the two subsystems are identical and  $C_s = C$ , the counter-propagating topological modes residing on either side of the contact interface perfectly cancel each other out [25]. In other words, the composite system becomes, by all means, a unified lattice domain encircled by a single chiral topological channel along its outer perimeter. A much more interesting regime however emerges when the two counter-propagating topological modes at the interface cannot mutually annihilate, i.e. if the two domains differ in a non-topological way such as an offset in the diagonal terms of the second subsystem Hamiltonian:  $H' = H + \delta\mathcal{I}$ . This constant on-site potential directly translates to a rigid shift of the entire quasi-energy spectrum of the affected domain by  $\delta$ . By way of an example, for  $\delta = \pi/T$ , the 0 and  $\pi$  bandgaps are effectively interchanged. The two counter-propagating topological states on either side of

the contact interface (green bands in the right subpanels of Fig. 2c) anti-cross, forming a pair of edge states residing in each bandgap (green bands in the left subpanel of Fig. 2c). Even though they are bi-directional, these curious entities inherit key aspects from the topology of the confining bulk media. As we discuss in more detail in the Supplementary, a topological description of TET states can be formulated by considering particular one-dimensional cuts in the dispersion relation of the composite system, which suggests that they indeed retain an increased robustness to disorder with respect to conventional trivial states. Surprisingly, TET states exist for any choice of the detuning  $\delta \neq 0$  (Fig. 2d), and readily interact with the chiral states of the outer perimeter. In the following, we will show how these interactions can be effectively used to inject and extract energy into and from topological edge states.

## 2 Experiments and results

We experimentally explore the behavior of TET states in detuned pairs of Kitagawa lattices formed by femtosecond laser-written waveguides [26] in a 150mm long fused silica chip. As a first step, we qualitatively demonstrate the existence of a bi-directional interface state and its ability to couple to the topological edge states (Fig. 3). Launching light into a single site along the outer perimeter serves to excite a topologically protected edge wave packet travelling in clockwise direction. Upon encountering the interface between the detuned domains, a fraction of its intensity is clearly captured by the TET state and subsequently routed downwards along the interface (Fig. 3a). When the initial excitation is instead placed on a site within the interface, a superposition of TET states is launched. These travel in both directions and eventually feed into the topological edge channel at both the upper and lower edges of the lattice (Fig. 3b). This experimentally observed behavior, illustrated in the top panels of Fig. 3, is faithfully reproduced by numerical tight-binding simulations, and unambiguously demonstrates that an interface between two different, yet topologically equivalent, anomalous Floquet topological insulators supports bi-directional states that are capable of interacting selectively with conventional topological edge channels.

In order to obtain more quantitative insights into the phenomenology of these unusual states, we devised a setting in which TET states can mediate interactions between topological edge states on opposite sides of a composite lattice (Fig. 4a). Here, light is first shunted out of the topological state at the upper edge, then conveyed a macroscopic distance  $d$  along the non-topological interface by the TET channel, and finally fed back into the topological state at the lower edge. In this vein, we implemented a series of L-shaped structures with different TET transport ranges  $d$  along the interface. For each of these structures, we launched single-site excitations of the topological state on the upper edge and subsequently detected the amount of light emerging at the bottom edge at the end of the sample. Notably, the lateral extent of the smaller of the two domains was

chosen such that the number of driving periods in the sample precludes any light from fully circumnavigating this region, so that any intensity detected along the bottom edge necessarily has to have traversed the lattice. This allows us to define the transmittivity  $T(d)$  as the fraction of the overall intensity found along the bottom edge.

After an initial drop-off, our tight-binding calculations show that, for a sufficiently long propagation time,  $T(d)$  eventually saturates towards a plateau value  $T_\infty > 0$  for  $d \rightarrow \infty$  (Fig. 4b). This conclusively demonstrates that the observed transmission is indeed mediated by a well-defined flow of light along the interface. In other words, TET states allow the population of topological edge channels to “tunnel” through the bulk without scattering. In addition to these numerical simulations, we developed a first-principle analytical model (details in the SI) that approaches the ideal curve in the high-order limit and accurately describes to what degree finite propagation times limit the overall transmission. Along with these calculations, our experimental results (Fig. 4c) indicate a finite asymptotic value of  $T$  for sufficiently strong detunings between the domains, i.e. for higher group velocities of the TET state. In contrast, as  $\delta$  is decreased, truncation of the transmitted wave packet precludes reliable measurements of  $T(d)$  for the system size at hand, and, as predicted by the analytical model and the finite-time tight binding calculations, the signature of the plateau is eventually lost. Such  $\delta$ -dependent behavior, observed also in the full numerical simulations (details see SI), is the signature of a slow-light regime achievable with small detunings, where the near-perfect cancellation of the counter-propagating interface states allows light to remain in the TET channel for extended periods of time as its group velocity approaches zero (Fig. 2d).

### 3 Conclusion

In this work, we introduced topology-entailed trivial states as novel paradigm for manipulating, interrogating and populating topologically protected currents without locally disrupting topology or resorting to higher-dimensional workarounds. The concept of TET states is general, as they can emerge at interfaces between topologically uniform domains that systematically differ by some conventional quantity, e.g. any non-zero offset between the otherwise homogeneous on-site energies of the two lattices. As such, these unusual hybrid entities are by definition topologically trivial, yet inherit important aspects of their topological origins, such as an increased robustness to disorder compared to conventional trivial states.

Our experiments in photonic Kitagawa-type anomalous topological insulator lattices clearly demonstrate the capability of TET states to locally interact with protected topological states of the outer perimeter in a bidirectional fashion, enabling both the deliberate extraction and injection of light from well-defined locations within the lattice. In a similar vein, we showed that TET states can act as long-range interconnects between spatially distinct topological channels that would otherwise be entirely isolated from one another.

By providing a readily tunable transport velocity, this *topological tunneling* also serves as flexible means to implement slow light on topological platforms. [27]. The applicative potential of TET-state based topological architectures is further bolstered by the comparable ease of design, and the possibility to evoke them on-demand by any number of mechanisms that can produce a transient shift in the on-site potential in a specific domain, e.g. by thermal [28, 29], electro-optic [30] or even nonlinear all-optical modulations [31].

## 4 Methods

### Numerical methods

Numerical simulations are performed with tight binding calculations run in MATLAB. The (2+1)D winding number of the time-evolution operator is defined from the k-space time-evolution operator as in [32],

$$\mathcal{W}_\epsilon = \frac{1}{8\pi^2} \int \text{Tr} \left( \mathcal{U}_\epsilon^{-1} \partial_t \mathcal{U}_\epsilon \left[ \mathcal{U}_\epsilon^{-1} \partial_{k_x} \mathcal{U}_\epsilon, \mathcal{U}_\epsilon^{-1} \partial_{k_y} \mathcal{U}_\epsilon \right] \right) dt dk_x dk_y$$

Where the operator  $\mathcal{U}_\epsilon$  is piecewise defined as follows:

$$\mathcal{U}_\epsilon(\mathbf{k}, t) = \begin{cases} U(\mathbf{k}, 2t) & t \in [0, T/2) \\ e^{-iH_{\text{eff}}^\epsilon(\mathbf{k})t} & t \in [T/2, T) \end{cases}$$

$U(\mathbf{k}, t) = \hat{\mathcal{T}} e^{-i \int H(\mathbf{k}, t) dt}$  is the time evolution operator,  $\hat{\mathcal{T}}$  is the time-ordering operator and  $H_{\text{eff}}^\epsilon = i/T \log(U)$  is the effective Floquet Hamiltonian. The branch cut for the logarithm of  $U$  allows to discriminate between 0 and  $\pi$  quasi-energy for the calculation of  $\mathcal{W}_\epsilon$ .

### Waveguide fabrication and characterization

Our photonic implementation of TET states was based on laser-written lattices of evanescently coupled waveguides [26]. Ultrashort laser pulses from a frequency doubled fiber amplifier system (Coherent Monaco) at a carrier wavelength of 517 nm were focused (50x objective, NA = 0.6) into the volume of 150 mm long fused silica samples (Corning 7980). The evanescent coupling rate between adjacent guides was controlled by modulating the distance between them, from a distance of 9  $\mu\text{m}$  for the coupling regions to 30  $\mu\text{m}$  for the regions without optical coupling. Cosine-shaped transitions were employed to connect the individual steps of the driving protocol into contiguous waveguide trajectories. In turn, the inscription speed served as process parameter to implement different propagation constants, i.e. the desired shift of the on-site potential. The waveguide arrangements were designed for an operating wavelength of 633 nm, and characterized by injecting light from a continuous-wave Helium-Neon laser light into specific lattice sites and subsequently imaging the output onto a CCD camera.

## 5 Acknowledgements

The authors would like to thank C. Otto for preparing the high-quality fused silica samples employed in this work. AS received partial funding from European Research Council (grant EPIQUS), Deutsche Forschungsgemeinschaft (grants SCHE 612/6-1, SZ 276/12-1, BL 574/13-1, SZ 276/15-1 and SZ 276/20-1) and the Alfried Krupp von Bohlen and Halbach foundation. FSP acknowledges fundings from Deutscher Akademischer Austauschdienst (grant 57507869 and 57381332). IC and FSP acknowledge financial support from the European Union H2020-FETFLAG-2018-2020 project "PhoQuS" (n.820392) and from the Provincia Autonoma di Trento, partly through the Q@TN initiative.

## 6 Author contributions

FSP, NS and ME fabricated the photonic waveguide systems. FSP, MK, ME, LJM and MH conducted the measurements and evaluated the data. FSP, MK and IC developed the theoretical description. FSP and MK conducted the numerical simulations. IC and AS supervised the work of their respective groups. All authors interpreted the results and co-wrote the manuscript.

## References

- [1] T. Ozawa, *et al.*, Topological photonics, *Rev. Mod. Phys.* **91**, 015006 (2019).
- [2] A. B. Khanikaev, *et al.*, Photonic topological insulators, *Nature Materials* **12**, 233–239 (2013).
- [3] F. D. M. Haldane, S. Raghu, Possible realization of directional optical waveguides in photonic crystals with broken time-reversal symmetry, *Physical Review Letters* **100**, 013904 (2008).
- [4] K. Fang, Z. Yu, S. Fan, Microscopic theory of photonic one-way edge mode, *Physical Review B - Condensed Matter and Materials Physics* **84**, 075477 (2011).
- [5] L. Lu, J. D. Joannopoulos, M. Soljačić, Topological photonics, *Nature Photonics* **8**, 821–829 (2014).
- [6] Z. Wang, Y. Chong, J. D. Joannopoulos, M. Soljačić, Observation of unidirectional backscattering-immune topological electromagnetic states, *Nature* **461**, 772–775 (2009).
- [7] M. C. Rechtsman, *et al.*, Photonic Floquet topological insulators, *Nature* **496**, 196–200 (2013).

- [8] M. Hafezi, S. Mittal, J. Fan, A. Migdall, J. M. Taylor, Imaging topological edge states in silicon photonics, *Nature Photonics* **7**, 1001-1005 (2013).
- [9] T. Ma, A. B. Khanikaev, S. H. Mousavi, G. Shvets, Guiding electromagnetic waves around sharp corners: Topologically protected photonic transport in metawaveguides, *Physical Review Letters* **114**, 127401 (2015).
- [10] A. B. Khanikaev, G. Shvets, Two-dimensional topological photonics, *Nature Photonics* **11**, 763–773 (2017).
- [11] K. Lai, T. Ma, X. Bo, S. Anlage, G. Shvets, Experimental realization of a reflections-free compact delay line based on a photonic topological insulator, *Scientific Reports* **6**, 28453 (2016).
- [12] G. G. Gentili, G. Pelosi, F. S. Piccioli, S. Selleri, Towards topological protection based millimeter wave devices, *Phys. Rev. B* **100**, 125108 (2019).
- [13] M. A. Bandres, *et al.*, Topological insulator laser: Experiments, *Science* **359**, eaar4005 (2018).
- [14] B. Bahari, *et al.*, Nonreciprocal lasing in topological cavities of arbitrary geometries, *Science* **358**, 636–640 (2017).
- [15] S. Ma, S. M. Anlage, Microwave applications of photonic topological insulators, *Applied Physics Letters* **116**, 250502 (2020).
- [16] I. Amelio, I. Carusotto, Theory of the coherence of topological lasers, *Phys. Rev. X* **10**, 041060 (2020).
- [17] S. Stützer, *et al.*, Photonic topological anderson insulators, *Nature* **560**, 461–465 (2018).
- [18] T. Kitagawa, E. Berg, M. Rudner, E. Demler, Topological characterization of periodically driven quantum systems, *Phys. Rev. B* **82**, 235114 (2010).
- [19] L. J. Maczewsky, J. M. Zeuner, S. Nolte, A. Szameit, Observation of photonic anomalous floquet topological insulators, *Nature Communications* **8**, 13756 (2017).
- [20] S. Mukherjee, *et al.*, Experimental observation of anomalous topological edge modes in a slowly driven photonic lattice, *Nature Communications* **8**, 13918 (2017).
- [21] A. Blanco-Redondo, B. Bell, D. Oren, B. J. Eggleton, M. Segev, Topological protection of biphoton states, *Science* **362**, 568–571 (2018).
- [22] S. Barik, *et al.*, A topological quantum optics interface, *Science* **359**, 666-668 (2018).



- [23] M. C. Rechtsman, *et al.*, Topological Protection of Photonic Quantum Entanglement, *2016 Progress in Electromagnetic Research Symposium (PIERS)* **3**, 974–974 (2016).
- [24] F. Klauck, M. Heinrich, A. Szameit, Photonic two-particle quantum walks in su-schrieffer-heeger lattices, *Photon. Res.* **9**, A1–A7 (2021).
- [25] J. Chen, W. Liang, Z.-Y. Li, Strong coupling of topological edge states enabling group-dispersionless slow light in magneto-optical photonic crystals, *Phys. Rev. B* **99**, 014103 (2019).
- [26] A. Szameit, *et al.*, Two-dimensional soliton in cubic fs laser written waveguide arrays in fused silica, *Optics Express* **14**, 6055–6062 (2006).
- [27] J. Guglielmon, M. C. Rechtsman, Broadband topological slow light through higher momentum-space winding, *Phys. Rev. Lett.* **122**, 153904 (2019).
- [28] F. Flamini, *et al.*, Thermally reconfigurable quantum photonic circuits at telecom wavelength by femtosecond laser micromachining, *Light: Science & Applications* **4**, e354 (2015).
- [29] Z. Chaboyer, T. Meany, L. G. Helt, M. J. Withford, M. J. Steel, Tunable quantum interference in a 3d integrated circuit, *Scientific Reports* **9**, 9601 (2015).
- [30] G. Li, K. A. Winick, A. A. Said, M. Dugan, P. Bado, Waveguide electro-optic modulator in fused silica fabricated by femtosecond laser direct writing and thermal poling, *Opt. Lett.* **31**, 739–741 (2006).
- [31] L. J. Maczewsky, *et al.*, Nonlinearity-induced photonic topological insulator, *Science* **370**, 701–704 (2020).
- [32] M. S. Rudner, N. H. Lindner, E. Berg, M. Levin, Anomalous edge states and the bulk-edge correspondence for periodically driven two-dimensional systems, *Phys. Rev. X* **3**, 031005 (2013).

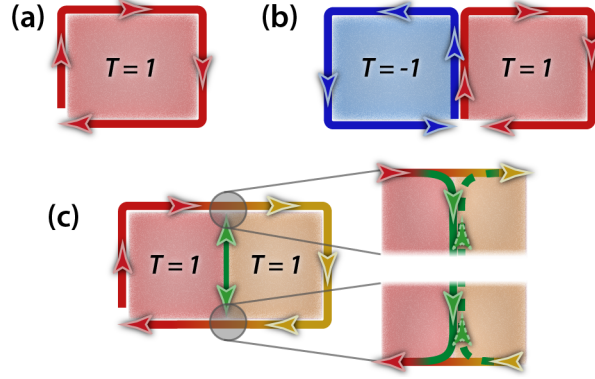


**Fig. 1: Topological, trivial, or both?** (a,b) Illustration of the Bulk-Edge correspondence principle for (a) a single topological insulator domain and (b) a composite of two topologically distinct materials. (c) Schematic illustration of a topologically homogeneous interface hosting topology-entailed trivial (TET) states. **inset** Examples of interaction between topological edge states and TET states (energy extraction and energy injection)

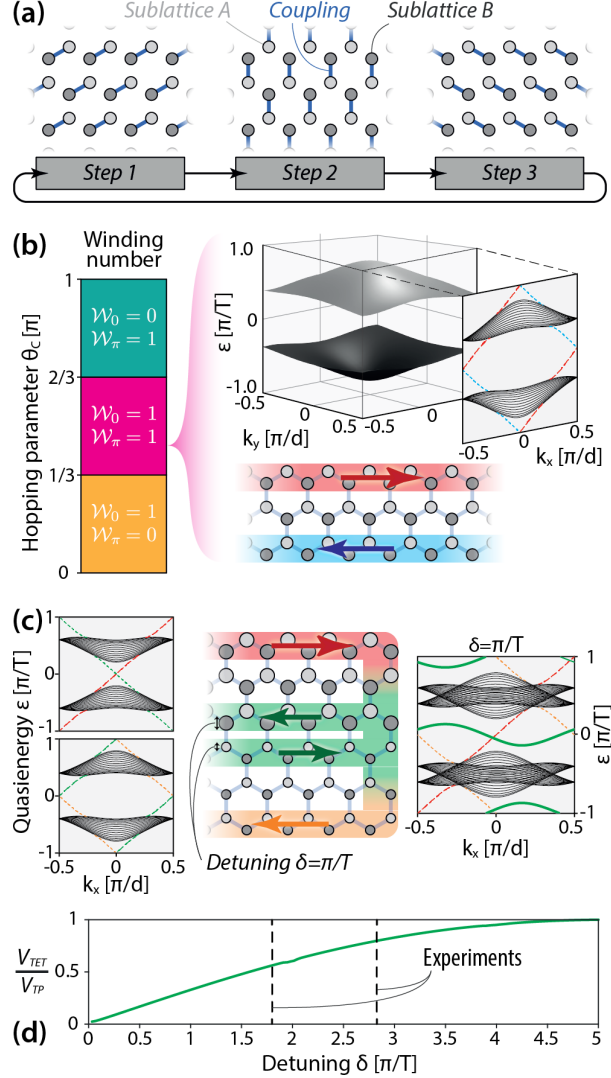


**Fig. 2: Synthesizing TET states.** (a) Schematic of the driving protocol for a Kitagawa model. Coupling along each of the lattice vectors is exclusively present in its dedicated step. (b) Left: Topological phase diagram of the system as a function of the coupling phase  $\theta_c = CT/3$ . Bi-directional TET interface states exist for  $1/3\pi \leq \theta_c \leq 2/3\pi$ , when the winding numbers of both gaps are 1. Right: Bulk band structure of the full Hamiltonian for  $\theta_c = 0.4\pi$ , and projected edge band structure of a semi-infinite ribbon with zig-zag edges on the  $x$  direction. Note that the topological states along the upper (red) and lower (blue line) edges propagate in opposite directions, in line with the slope of their respective branches in the dispersion relation along  $k_y$ . (c) Center: Schematic of a composite system of two detuned but otherwise identical Kitagawa model-domains in direct contact along the zigzag edge. For a detuning of  $\delta = \pi/T$ , the band

structures of the isolated domains (Left) are shifted by half a Floquet unit cell with respect to one another. Right: Band structure of the hybrid system. The counter-propagating topological states localized at the interface hybridize into a pair of TET states (thick green lines). **(d)** Group velocity of TET states relative to topological edge states as a function of the relative detuning  $\delta$  for coupling phase  $\theta_c = \pi/2$ .

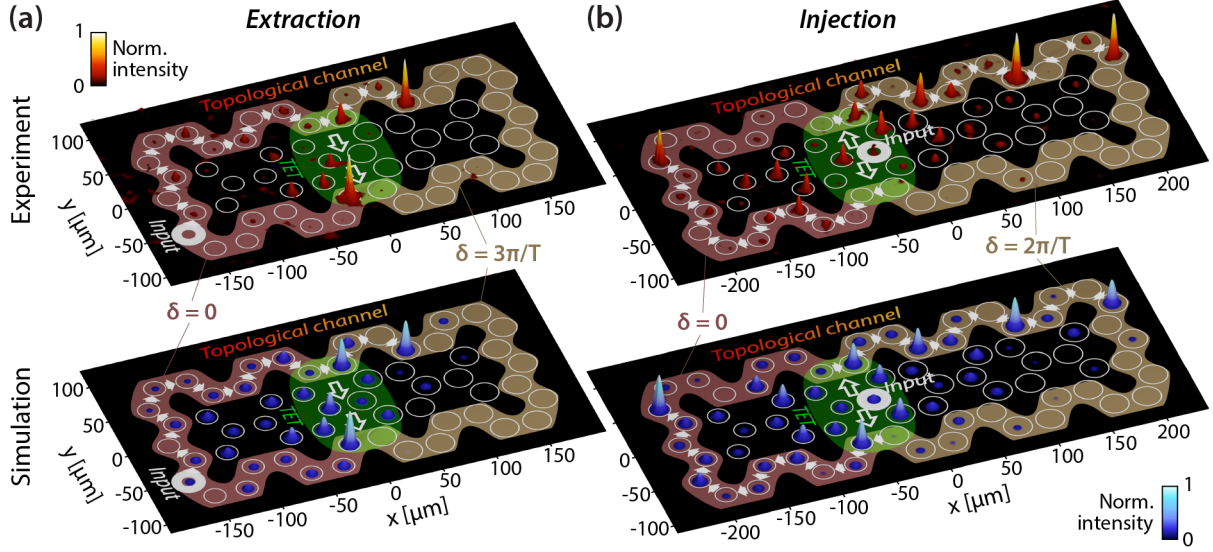


**Fig. 3: Accessing protected channels without compromising their topology.** Qualitative demonstration of the extraction (a) and injection (b) of energy from/into a topological mode by a TET state. In both cases the excitation is performed on a single site and the output intensity is recorded after a propagation of 7 (left) and 8 (right) driving periods  $T$ , respectively. The system on the left contains an interface with  $\delta = 2\pi/T$ , while the interface of the right system features a detuning of  $\delta = 3\pi/T$ . Top: Observed intensity distribution in the output facet of the waveguide lattices. Bottom: Corresponding tight-binding simulations.

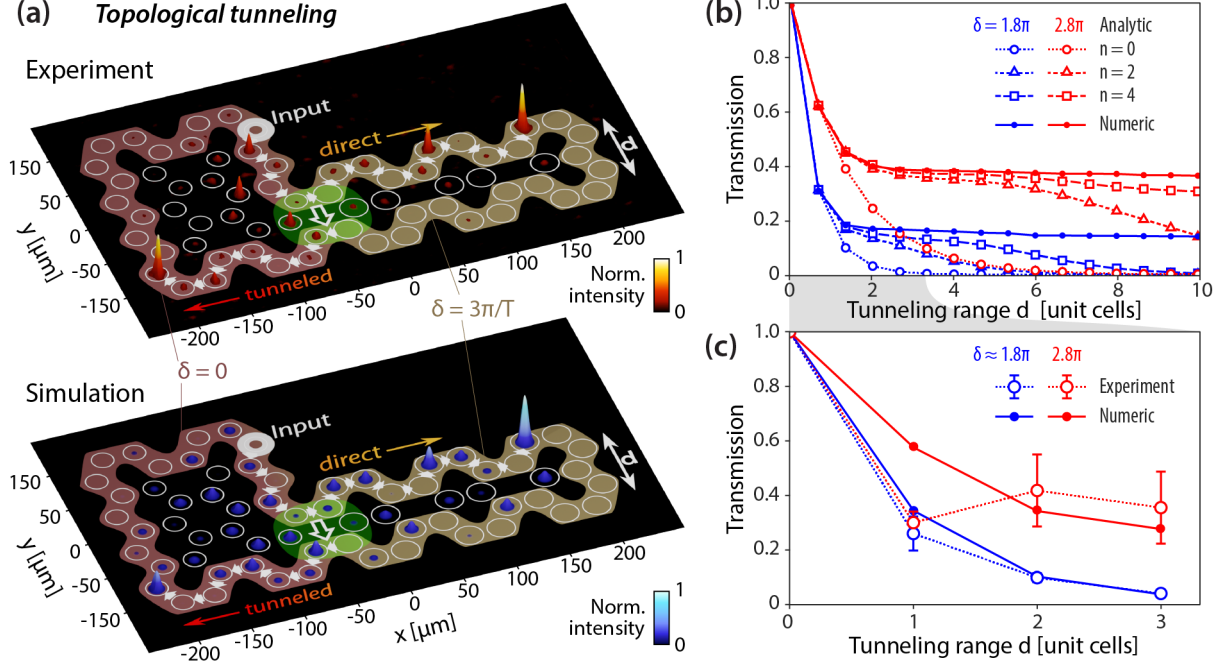


**Fig. 4: Topological tunneling.** (a) Observed (top) and simulated (bottom) intensity distribution at the output facet for an interface length  $d = 2$  after a propagation of 7 driving periods. (b) Transmission  $T$  as a function of the tunneling range  $d$  calculated from a truncated analytical model (empty marks) at order  $n$  and numerical tight-binding simulation (filled circles) of a 50 periods propagation, respectively. All the curves are relative to a system with  $\theta_c = \pi/2$ . (c) Measurements (empty circles) and tight-binding simulations (filled circles) of the transmission  $T$  for the fabricated structures, after a propagation over 7 periods. Tight-binding simulations are performed using a fitted value of  $\theta_c = 0.4\pi$  for the coupling phase. Lines in panels (b,c) are included as a guide to the eye.

# Populating and probing protected edge states through topology-entailed trivial states

Supplementary Informations

## ANALYTICAL MODEL FOR TOPOLOGICAL TUNNELING

In this section we discuss the derivation of the analytical model developed to support the observation of the transmission plateau discussed in figure 4 of the main manuscript. Even though we will not be able to completely solve the problem, a truncated expansion will already provide interesting insights on the numerical and experimental observations.

The time dependent  $\mathbf{k}$ -space Hamiltonian of an Anomalous Floquet Honeycomb lattice, as already discussed in the main text, can be written as:

$$H(\mathbf{k}, t + T) = H(\mathbf{k}, t) = \sum_{i=1}^3 \mathbb{1}_{T_i}(t) \begin{pmatrix} 0 & C e^{j\mathbf{k} \cdot \mathbf{b}_i} \\ C e^{-j\mathbf{k} \cdot \mathbf{b}_i} & 0 \end{pmatrix} \quad (1)$$

In order to build an easily interpretable analytic model in the following we will restrict to  $\theta_c = CT/3 = \pi/2$ . In this condition the hopping between two coupled sites is complete and the bulk bands of the Kitagawa model are flat. Topological edge states extend across the entire Energy Brillouin zone and the system is an Anomalous Floquet insulator with all bulk states fully localized. Our specific choice of  $\theta_c$  does not limit the observed physics but implies the comfortable condition of the interface states being completely localized in the edge lattice sites and not leaking with their exponential tails into the bulk of their confining lattices (fig S1 a). Furthermore such condition is the design goal of the experimental implementation and is the middle point of the Anomalous Floquet topological phase such that unavoidable imperfections in the fabrications are least likely to cause a topological phase transition to a non-anomalous regime. Our experimental implementation of the Anomalous Floquet honeycomb lattice is essentially based on the realization of a network of directional couplers, where every coupling step consists in a directional coupler with given coupling strength, length, and relative detuning between the coupled waveguides. If we assume that the coupling between tuned waveguides is complete we can model the interface as a ladder of directional couplers (fig S1b). The ladder rails are tuned directional couplers with complete hopping supporting unidirectional states that propagate with opposite directions (because of the way we alternate the couplings in time), while the rungs of the ladder are de-tuned directional couplers with a given reflection (diagonal terms in the matrix) and transmission (off-diagonal terms) coefficients.

In the whole ladder we can identify 3 different couplers, with their correspondent color codes as in figure S1 b: 100% couplers on the left side (orange), 100% couplers on the right side (red) and de-tuned couplers (purple). Having defined  $(A, B)$  the light amplitude in the two waveguides of the de-tuned directional coupler, the coupled mode formalism allows to retrieve the transmission matrix

$$T_1(z) = \begin{pmatrix} \alpha(z, \tilde{\delta}, \sigma) & \beta(z, \tilde{\delta}, \sigma) \\ \beta(z, \tilde{\delta}, \sigma) & \alpha^*(z, \tilde{\delta}, \sigma) \end{pmatrix} e^{-i\tilde{\delta}z}, \quad (2)$$

where  $z$  is the length of the coupler,  $\alpha(z, \tilde{\delta}, \sigma) = \cos(\sigma z) + i\frac{\tilde{\delta}}{\sigma} \sin \sigma z$ ,  $\beta(z, \tilde{\delta}, \sigma) = -i\frac{C}{\sigma} \sin \sigma z$ ,  $\sigma = \sqrt{\tilde{\delta}^2 + C^2}$  and  $\tilde{\delta} = \frac{\delta C}{3\pi}$ , where  $\delta$  is the global energy offset between the two subsystem discussed in the main manuscript. The transmission matrix relates the light intensity present in the two waveguides as a function of the directional coupler length and the injected light:

$$\begin{pmatrix} A(z) \\ B(z) \end{pmatrix} = T_1(z) \begin{pmatrix} A_0 \\ B_0 \end{pmatrix} \quad (3)$$

Since the length of the directional coupler is fixed by our experimental implementation in order to realize complete hopping in the tuned case, we fix  $z = l_c = \pi/(2C)$ . We can now rewrite the transmission matrix of the detuned directional coupler with fixed length  $l_c$  as:

$$T_{1,l_c} = \begin{pmatrix} \alpha(\Theta) & \beta(\Theta) \\ \beta(\Theta) & \alpha^*(\Theta) \end{pmatrix} e^{-i\frac{\delta}{6}} \quad (4)$$

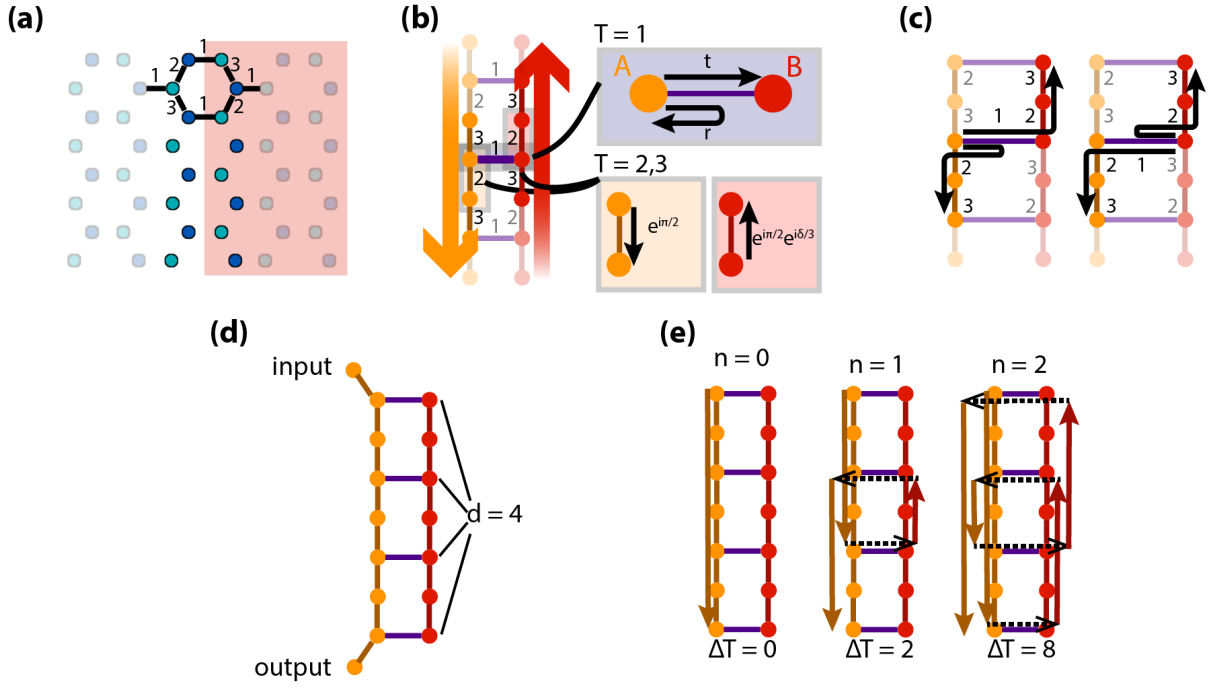


Fig. S1. **(a)**: If the diagonal modulation steps (labeled 2,3) provide 100% coupling, light hops only between reticular sites that are closest to the interface. Therefore the interface can be considered as a quasi 1D directional coupler ladder. **(b)**: Schematic of the directional coupler ladder. Horizontal couplers (purple) are detuned therefore they present both a transmission and a reflection coefficient whereas the vertical couplers are complete hence they only have a transmission coefficient (with a phase dependent on the relative energy detuning). The numbers indicate the sequence with which the coupling steps are modulated in time. **(c)**: Schematic of the only two possible transport paths within a driving period for light initially located on the left(right) sites of the de-tuned coupler. **(d)**: Schematic of a ladder with finite length  $d$  **(e)**: Examples of order 0, 1 and 2 paths with the relative delay of their output  $\Delta T$ .

Having defined  $\alpha(\Theta) = \cos(\frac{\pi}{2}\Theta) + i\frac{\delta}{3\pi}\frac{\sin\frac{\pi}{2}\Theta}{\Theta}$ ,  $\beta(\Theta) = -i\frac{\sin\frac{\pi}{2}\Theta}{\Theta}$  and  $\Theta = \sqrt{(\frac{\delta}{3\pi})^2 + 1}$  as an unbounded parameter  $\Theta \geq 1$  with  $\Theta = 1$  iff  $\delta = 0$ . The matrix elements of  $T$  are only determined by a particular choice of  $\delta$ . In case we inject light only on the left waveguide (A) of the detuned directional coupler we can then define two parameters:

$$r = \alpha(\Theta)e^{-i\frac{\delta}{\Theta}}, \quad \text{and} \quad t = \beta(\Theta)e^{-i\frac{\delta}{\Theta}} \quad (5)$$

that defines the amplitude of the *reflected* and *transmitted* light by the detuned interface coupler. It is easy to verify that  $|r|^2 + |t|^2 = 1$ .

After a first coupling step in which only the detuned coupler is active (fig. S1 b top inset), the successive two coupling steps happen only in correspondence to the sides of the ladder, on which the coupling is complete (fig. S1 b bottom inset). If we consider light initially localized on the left waveguide of a detuned directional coupler, after an entire modulation period, composed by the sequence of one detuned coupler and two balanced couplers, the light intensity will be in part transported one unit cell down, via the left rail topological mode, and the remaining part will be transported one unit cell upwards via the right rail topological mode (fig. S1 c), the corresponding coefficients can be calculated as the product of the three couplers involved:  $t_l = -\beta(\Theta)e^{-i\frac{\delta}{\Theta}}e^{-i2\frac{\delta}{3}}$  for the upwards transmission and  $r_l = -\alpha(\Theta)e^{-i\frac{\delta}{\Theta}}$  for the downwards transmission. Analogously one can define  $r_r$  and  $t_r$  coefficients for light initially localized on the right (B) waveguide of the detuned coupler. If one wants to study the dynamics in an interface of finite length  $d$  it is necessary to consider a chain of all these elementary transmissions.

Let's consider a finite interface of length  $d$ , where  $d$  is the number of de-tuned directional couplers present in the interface (as in fig. S1 d). If light is initially injected in the top-left waveguide of the interface and one waits a sufficient amount of time all the light will exit the interface either from the bottom topological output or from the top topological output. Let's consider light that travels through the entire interface and exits on the bottom side. To calculate such portion of light we need to consider all the possible paths that can be followed to go from the top left to the bottom left waveguides. We decide to divide such paths in families according to how many times light is coupled



from the left to the right side of the interface (and backwards) (see fig.S1 e). We analyse such paths separately.

$n = 0$ : Let's index the de-tuned couplers with  $k = 0..d - 1$ . If light never crosses the interface then it reflects  $d$ -times on each of the de-tuned couplers and the transmission coefficient is simply the product of all the  $r_l$ :

$$A_0 = r_l^d = \left(-\alpha(\Theta)e^{-i\frac{\delta}{6}}\right)^d \quad (6)$$

Of course it exists only one path of this kind, and it contributes to an output that is delayed of  $T = d$  modulation periods after injecting light on the upper-left waveguide of the interface. As this is the quickest possible path, we define as  $\delta T = 0$  the time delay caused by the direct path. We here note that such transmission coefficient decays exponentially to zero for  $d \rightarrow \infty$ . This means that higher order paths must contribute to the "tunneled output".

$n = 1$ : Let's now consider all the paths that cross the interface once from left to right (and thus once from right to left). The first crossing (left to right) can happen at any given point  $c_1 \in [1, d - 1]$ , while the second crossing (right to left) at any given point  $c'_1 \in [0, c_1 - 1]$ . The amplitudes of such paths are given by

$$\begin{aligned} A_1(c_1, c'_1) &= r_l^d (\beta^2 e^{-i\delta}) \left(|\alpha|^2 e^{-i\delta}\right)^{c_1 - c'_1 - 1} \\ &= r_l^d R_1 P_1^{c_1 - c'_1 - 1} \end{aligned} \quad (7)$$

Where  $R_1 = \beta^2 e^{-i\delta}$  is the transmission term for a "loop" that is a double transmission from left to right and from right to left, while  $P_1 = |\alpha|^2 e^{-i\delta}$  is the transmission term for a propagation of 1 unit cell in the right side of the interface (and a corresponding propagation of 1 unit cell on the left side). To account for the contribution of all such paths it is necessary to sum over all values of  $c_1$  and  $c'_1$ :

$$\mathcal{A}_1 = r_l^d R_1 \sum_{c_1=1}^{d-1} \sum_{c'_1=0}^{c_1-1} P_1^{c_1 - c'_1 - 1} = r_l^d \frac{R_1}{P_1} \sum_{c_1=1}^{d-1} \sum_{c'_1=0}^{c_1-1} P_1^{c_1 - c'_1} \quad (8)$$

As a crossing of the interface takes one modulation period, plus two modulation periods for every propagation step on the right side of the interface (one on the right side and one on the left side) the time delay of these paths can be calculated as  $\Delta T(A_1(c_1, c'_1)) = 2(c_1 - c'_1)$ . Moreover we note that all the paths arriving at the same time sum up coherently as the phase depends only on  $(c_1 - c'_1)$ .

$n = 2$ : In general, a particular second order path will be characterized by four crossings happening at four points  $c_1 c'_1 c_2 c'_2$ , where, as before  $c_1 \in [1, d - 1]$  and  $c'_1 \in [0, c_1 - 1]$ . The third and fourth crossings can happen in  $c_2 \in [c'_1 + 1, d - 1]$  and  $c'_2 \in [0, c_2 - 1]$ . The amplitude of any particular second order path is given by:

$$\begin{aligned} A_2(c_1, c'_1, c_2, c'_2) &= r_l^d (\beta^2 e^{-i\delta}) \left(|\alpha|^2 e^{-i\delta}\right)^{c_1 - c'_1 - 1} (\beta^2 e^{-i\delta}) \left(|\alpha|^2 e^{-i\delta}\right)^{c_2 - c'_2 - 1} \\ &= r_l^d R_1^2 P_1^{c_1 - c'_1 - 1} P_1^{c_2 - c'_2 - 1} \\ &= r_l^d \left(\frac{R_1}{P_1}\right)^2 P_1^{c_1 - c'_1} P_1^{c_2 - c'_2} \end{aligned} \quad (9)$$

Therefore the sum of all the contributions given by second-order paths can be found by summing over all coefficients:

$$\mathcal{A}_2 = r_l^d \left(\frac{R_1}{P_1}\right)^2 \sum_{c_1=1}^{d-1} \sum_{c'_1=0}^{c_1-1} \sum_{c_2=c'_1+1}^{d-1} \sum_{c'_2=0}^{c_2-1} P_1^{c_1 - c'_1} P_1^{c_2 - c'_2} \quad (10)$$

As for the previous case, the arrival times of such paths can be written as  $\Delta T(A_2(c_1, c'_1, c_2, c'_2)) = 2(c_1 + c_2 - c'_1 - c'_2)$ . Repeating the reasoning allows to retrieve the general expression of the output for the  $n$ -th order path, involving a summation over  $2n$  indexes  $\underline{c}, \underline{c}' = \{c_i, c'_i\}_{i=1:n}$ :

$$\mathcal{A}_n = r_l^d \left(\frac{R_1}{P_1}\right)^n \sum_{\underline{c}, \underline{c}'} \prod_{i=1}^n P_1^{c_i - c'_i} \quad (11)$$

Since different paths contribute to the output at different times, in general the tunneled output will be highly dispersed. The transmission is given by the ratio between the total output intensity and the injected intensity.

Assuming we inject a unitary intensity, the transmission will be the sum of the intensities at the output of the interface at every time instant:

$$\mathcal{T} = \sum_{\Delta T=0}^{\infty} |O(\Delta T)|^2 \quad (12)$$

The *instantaneous output*  $O(\Delta T)$  denotes the light intensity, taking into account all order paths, leaking in the bottom topological mode at each time instant  $\Delta T$  following the quickest path (the 0-th order). We can write this term as a coherent sum of contributions from all orders:

$$O(\Delta T) = \sum_{n=0}^{\infty} O_n(\Delta T) \quad (13)$$

We now denote  $\Delta T_i$  the delay caused by the  $i$ -th crossing of a generic path. As an order- $n$  path implies exactly  $n$  crossings  $\{\Delta T_i\}_{i=1:n}$  partitions  $\Delta T$  in exactly  $n$  parts ( $\sum_{i=1}^n \Delta T_i = \Delta T$ ). Since  $\Delta T_i = 2(c_i - c'_i)$  is even, also  $\Delta T = 2t^*$  has to be even. We can rewrite  $O_n(\Delta T)$  as:

$$O_n(2t^*) = O_n(\Delta T) = r_l^d \left( \frac{R_1}{P_1} \right)^n \sum_{\Delta T_1 \dots \Delta T_{n-1}} \sum_{c_1 \dots c_n} P_1^{t^*}, \text{ where } t^* \in \mathbb{N} \quad (14)$$

Where,  $1 \leq \Delta T_i \leq 2t^* - \sum_{k=1}^{i-1} \Delta T_k - (n-i)$ , and  $\max(c_{i-1} - \Delta T_{i-1} + 1, \Delta T_i) \leq c_i \leq d-1$ . We observe that the instantaneous output has contribution only for even time-delays  $\Delta T = 2t^*$  and if expanded at the  $n$ -th order is exact for time delays  $\Delta T \leq 2n$ . The solution of the problem has a strictly combinatorial nature relying in finding a closed form for the (integer) path number  $\mathcal{N}$  on each order and time-delay  $\Delta T$ . We can indeed re-write the previous as:

$$O_n(2t^*) = r_l^d \left( \frac{R_1}{P_1} \right)^n P_1^{t^*} \mathcal{N}(d, n, t^*) \quad (15)$$

Where  $\mathcal{N}(d, n, t^*)$  encapsulates a sum over  $2n-1$  coefficients ( $c_1 \dots c_n$  and  $T_1 \dots T_{n-1}$ ) subject to the aforementioned bounds.

Symbolic calculations show that  $\mathcal{N}(d, n, t^*)$  always diverge for  $d \rightarrow \infty$ . However calculating the coherent sum between two consecutive-order contributions with the same time delay one gets:

$$O_n(2t^*) + O_{n+1}(2t^*) = r_l^d P_1^{t^*} \left( \frac{R_1}{P_1} \right)^n \left( \mathcal{N}_n + \frac{R_1}{P_1} \mathcal{N}_{n+1} \right) = r_l^d P_1^{t^*} \left( \frac{R_1}{P_1} \right)^n \left( \mathcal{N}_n - \frac{|\beta|^2}{|\alpha|^2} \mathcal{N}_{n+1} \right) \quad (16)$$

Therefore the relative strength of successive order contributes is at the basis of the non-diverging behaviour of  $\mathcal{T}(d)$  for  $d \rightarrow \infty$ . This implies that truncating the analytical model to a finite order causes an increasingly big error for the instantaneous output corresponding to longer interfaces. On the bright side, we note that the  $n$ -th order path contributes to the instantaneous output only for  $t^* \geq n$ , therefore the instantaneous output is exact for  $\Delta T < 2n$  and by truncating both the expansion order and the maximum propagation time we are able to obtain physically meaningful results well-agreeing with the experimental observations and that approaches the numerical simulation for increasing order expansion.

## FURTHER NUMERICAL SIMULATIONS

In the main text we claim that the transmission decay observed in the experimental results and predicted by numerical simulation results from the reduced group velocity of TET states in systems characterized by a small detuning. Indeed the results presented in figure 2d of the main text show that topological edge states, for  $\theta_c = \pi/2$ , exist for any choice of the relative detuning  $\delta$ , with a group velocity increasing with  $\delta$ . The group velocity dependence on the relative detuning can be intuitively understood from the bandstructure zoology presented in figure S2. As it is clearly observable, TET states are always bounded by the bulk bands of the two subsystem, and appear in the quasi-energy region interested by the gap interchange. As this region becomes bigger with increasing  $\delta$ , the same does the TET state bandwidth hence increasing the maximum slope of the state.

The analytical model shows that when the interface depth  $d$  grows, the dominant contributions to the output are the higher order ones, which inherently arrive at a later time because of the delay caused by crossing the interface

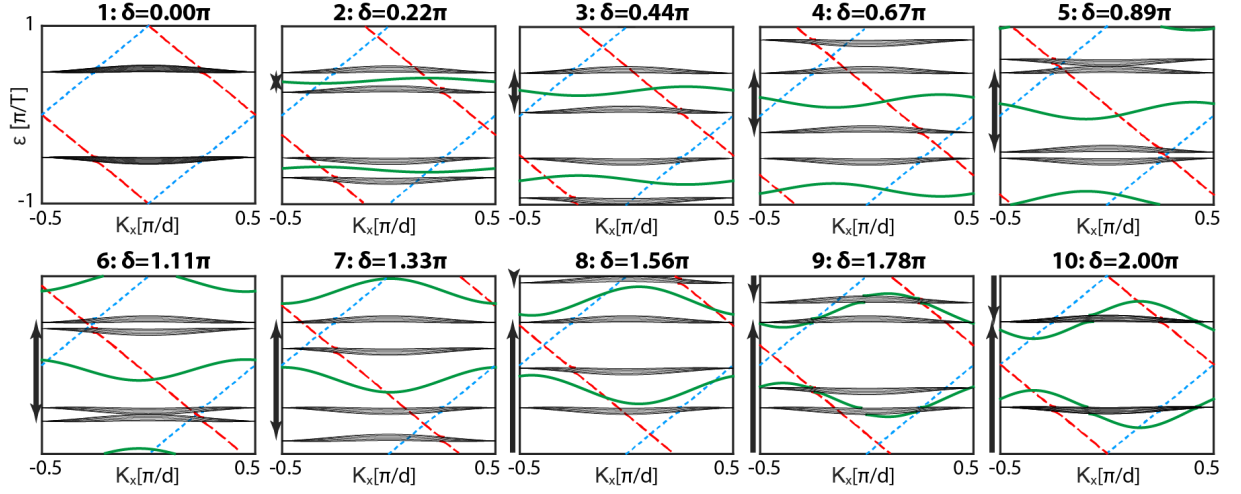


Fig. S2. Interface bandstructures for various values of the relative detuning  $\delta$ . All the plots are calculated considering a coupling constant  $\theta_c = 0.47\pi$  and 5 unit cells on each side of the interface. The arrows on the left side of each plot shows the graphical interpretation of the energy detuning, i.e. the energy shift of the right side interface bulk bands. dashed red lines are topological states localized on the right edge, dotted blue lines are topological states localized on the left edge while continuous green lines are TET states localized at the interface. Note that in plots number 8-10 the energy shift  $\delta > 3\pi/2$  causes a winding of the *common bandgap* region around the quasi-energy brillouin zone.

multiple times. As a matter of fact, truncating the propagation after few modulation steps will inevitably cause a decay of the output intensity for longer interface lengths  $d$ , and such decay will be more evident for smaller detunings  $\delta$ . This effect is illustrated in figure S3 (a,b) where we plot the numerical calculation of the instantaneous output of interfaces with relative detunings of  $1.8\pi$  and  $2.8\pi$ . Comparing curves describing the same interface length on the two subpanels it is evident that the transmission peak comes at a later time for smaller detunings, which reflects the lower group velocity of the wavepacket. In a practical experiment the total output is the integral of the instantaneous output up to a maximum time delay  $T_{max}$  defined by the experimental implementation. If the observable time span is too small, the wavepacket is truncated and the transmission plateau cannot be observed (fig S3 c).

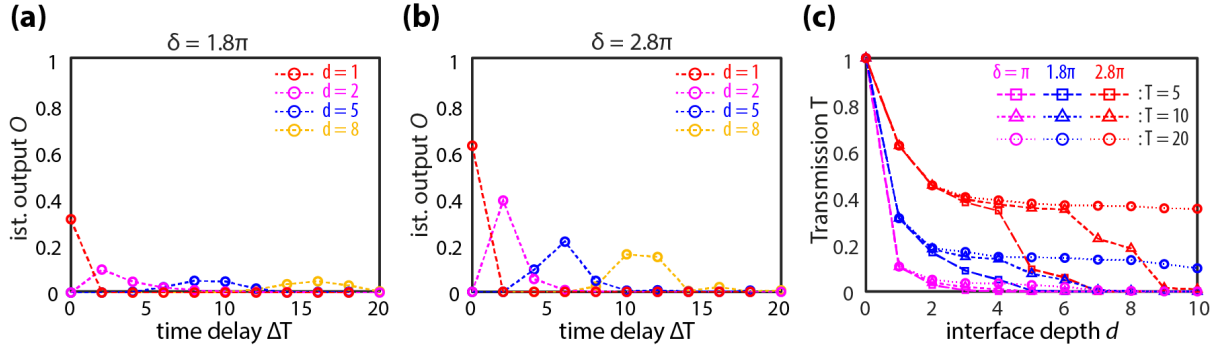


Fig. S3. **(a,b)**: Instantaneous output for an interface of varying depth  $d$  and relative detuning  $1.8\pi$  (a) and  $2.8\pi$  (b). Note that the  $O(\Delta T)$  has contribution only for even time delays, as described in the previous section. **(c)**: Numerical simulation of the transmission  $T(d)$  after a short propagation time.

The possibility to tune the propagation properties of interface states such as their speed is an important feature of our model. Furthermore the existence of TET states for wide range of parameters is an important signature of their topological origin. In figure S4 we plot the group velocity of bi-directional interface states as a function of the relative detuning between two subsystems and the coupling phase within both of the subsystems, normalized to the group velocity of edge topological states. The results show that TET states with a comparably low group velocity exist within essentially the entire parametric region in which the bulk lattices are in the Anomalous Floquet Topologically Insulating (AFTI) phase (delimited by the green dashed lines). Importantly, we note the appearance of certain parametric regions in which the lattices are in the A-FTI phase but no states are found (missing colors). This feature

is peculiar of our study model, and is due to the increased bulk band dispersion for  $\theta_c \approx \pi/3$  or  $\theta_c \approx 2\pi/3$  which effectively decreases the quasi-energy region in which TET states can appear (cfr. figure S2). Moreover, observing figure S4 one may note the appearance of fast interface states in the parametric region  $\theta_c \geq 2\pi/3$ . Those states stems from the hybridization of trivial bi-directional states which are supported by the zig-zag termination of a honeycomb lattice therefore their origin is not topological.

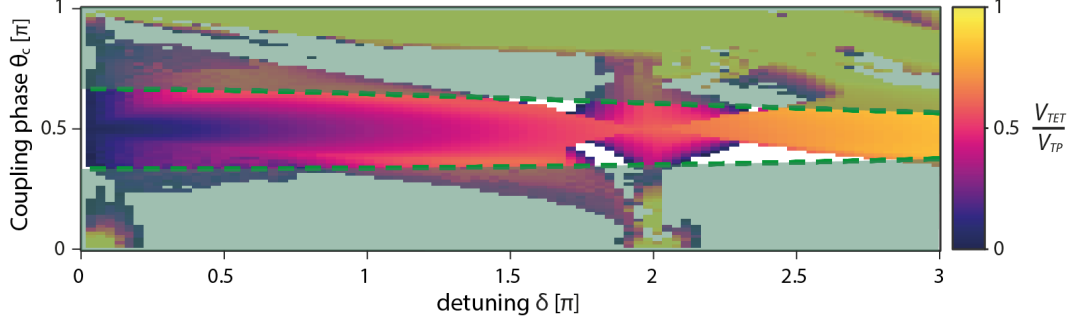


Fig. S4. Group velocity of bi-directional interface states, normalized to the group velocity of topological edge states, for different values of the subsystem detuning  $\delta$  and coupling phase  $\theta_c$ . Shaded areas correspond to parametric regions in which the underlying model is not in the Anomalous Floquet topological phase. The fast bi-directional interface states found for  $\theta_c \geq 2\pi/3$  derive from the hybridization of trivial bi-directional states supported by the zig-zag termination of a honeycomb lattice.

## A TOPOLOGICAL ARGUMENT ON TET STATE PROTECTION

In the main manuscript we argue that TET states are fundamentally different from conventional trivial states that may be found e.g. at the interface between two trivial insulators. A conceptual reason for that is that TET states are obtained by a superposition between counterpropagating topological states, therefore whatever mechanism (to which topology is unaltered) that may destroy such superposition would immediately restore topological propagation in the affected region. As topological propagation is insensitive to localization such defect, as for instance missing or heavily detuned interface sites, or even randomly distributed noise across the whole interface, would not be able to localize light flowing in TET states.

In this section we provide a topological argument that links the existence of interface TET states to a topological invariant of the bulk AFTIs therefore allowing to predict TET states via the bulk-edge correspondence principle. To this purpose we study the parametric 1D Floquet operator  $\mathcal{U}_{k_y}(k_x)$  derived from the full 2D Floquet operator  $\mathcal{U}(k_x, k_y)$  by fixing the value of  $k_y$  (aligned to the direction of the topologically homogeneous interface). We then demonstrate that, for specific values  $k_y = 0$  and  $k_y = \pi/2$ , the 1D interface between dimensionally reduced Floquet operators  $\mathcal{U}_{k_y}(k_x)$  with "interchanged bandgaps" ( $\delta = \pi/T$ ) supports 0D interface states protected by the chiral symmetry of  $\mathcal{U}_{k_y}(k_x)$ . Even though the provided treatment is valid only for the interchanged bandgap case, in which the relative detuning between the two systems is  $\delta = \pi/T$  only and it does not yet explain how to connect the protected 0D interface states to the 1D TET states, still it does provide an interesting insight on how the appearance of TET states might be rooted in the subsystems non-trivial topology.

The lattice is described by a piecewise constant Hamiltonian  $H$  that can be divided into three subsequent matrices  $H_i$  corresponding to the three modulation steps. In Bloch invariant form and choosing a unit cell that has the same symmetry of a zigzag edge (an analogous construction can be carried out for the bearded and armchair edge, but we restrain our analysis to that specific geometry) the k-space Hamiltonians take the following form:

$$\begin{aligned} H_1 &= C \begin{pmatrix} 0 & e^{-i(q_x+q_y)} \\ e^{i(q_x+q_y)} & 0 \end{pmatrix} = C \cos(q_x + q_y)\sigma_1 + C \sin(q_x + q_y)\sigma_2 \\ H_2 &= C \begin{pmatrix} 0 & 1 \\ 1 & 0 \end{pmatrix} = C\sigma_1 \\ H_3 &= C \begin{pmatrix} 0 & e^{-iq_y} \\ e^{iq_y} & 0 \end{pmatrix} = C \cos(2q_y)\sigma_1 + C \sin(2q_y)\sigma_2 \end{aligned}$$

Where  $\sigma_i$  are Pauli matrices and  $q_x = 3k_x/2$ ,  $q_y = \sqrt{3}k_y/2$ , with  $q_x \in [-\pi; \pi]$  and  $k_y \in [-\pi/2; \pi/2]$ , parametrize the whole Brillouin zone.

The Fourier-transformed Floquet operator  $\mathcal{U}(q_x, q_y)$  is defined as  $\mathcal{U}(q_x, q_y) = U(T, 0) = \mathcal{T}e^{-i \int_0^T H(q_x, q_y, t) dt}$ , being  $U(t_2, t_1)$  the time evolution operator from time  $t_1$  to  $t_2$ ,  $\mathcal{T}$  the time-ordering operator and  $T$  the whole driving period. Let's here note that it is possible to define a whole class of operators  $\mathcal{U}_\tau(q_x, q_y)$  defined as  $\mathcal{U}_\tau(q_x, q_y) = U(T + \tau, \tau) = \mathcal{T}e^{-i \int_\tau^{T+\tau} H(q_x, q_y, t) dt}$ , which differs among each other only accordingly to the starting time  $\tau$  of the driving. Since the driving is periodic, such operators are related to  $\mathcal{U}$  by a similarity transformation  $U^{-1}(\tau, 0)\mathcal{U}_\tau U(\tau, 0) = \mathcal{U}$  hence they share the same eigenvalues. This means that, as long as the bandstructure is concerned, the Floquet operator can be arbitrarily defined by choosing any time instant as the starting point for the *time-unit cell*. However in general the properties of  $\mathcal{U}$  might depend on a specific choice of  $\tau$ .

First, we take into account the family of 1D Floquet Operators  $\mathcal{U}_{\tau, q_y}(q_x)$ , obtained from  $\mathcal{U}_\tau(q_x, q_y)$  by fixing a specific value for  $q_y$ . Then we study the topological properties of such operators in terms of Winding Numbers. In particular, following the treatment in [1, 2], we are interested in a form of  $\mathcal{U}_{\tau, q_y}(q_x)$  such that the full Floquet operator can be decomposed into two half period operators  $A_{q_y}(q_x)$ ,  $B_{q_y}(q_x)$  related by a chirality transformation

$$\begin{aligned} \mathcal{U}_{\tau, q_y}(q_x) &= B_{q_y}(q_x) \cdot A_{q_y}(q_x) \\ \Gamma^\dagger A_{q_y}(q_x) \Gamma &= B_{q_y}^\dagger(q_x), \text{ with arbitrary } \Gamma \end{aligned} \quad (17)$$

If such representation can be found than  $A_{q_y}(q_x)$  can be written as:

$$A_{q_y}(q_x) = \begin{pmatrix} \alpha(q_x) & \beta(q_x) \\ \gamma(q_x) & \delta(q_x) \end{pmatrix}$$

With  $\alpha, \beta, \gamma, \delta$  complex function of a single variable  $q_x$ , parametrized in  $q_y$ . If  $\mathcal{U}$  is gapped both at  $\epsilon = 0$  and  $\epsilon = \pm\pi$  (Anomalous Floquet Topological phase), the winding number of  $\alpha(q_x)$  corresponds to the number of 0D edge states at  $\epsilon = 0$  and specific  $q_y$  while the winding number of  $\beta(q_x)$  corresponds to the 0D edge states at  $\epsilon = \pi$  and specific  $q_y$ .

Among all possible choices for the time-unit cell, the most practical one is using  $\tau = \frac{T}{6}$ , hence considering the middle of the first modulation step as the initial time instant. The corresponding Floquet operator takes the following form

$$\mathcal{U}_{\frac{T}{6}, q_y}(q_x) = U\left(\frac{T}{6}, 0\right) U\left(T, \frac{2T}{3}\right) U\left(\frac{2T}{3}, \frac{T}{3}\right) U\left(\frac{T}{3}, \frac{T}{6}\right) \quad (18)$$

Using the matrix representations of the Hamiltonians and the definition of  $U(t_2, t_1)$  we get:

$$\mathcal{U}_{\frac{T}{6}, q_y}(q_x) = e^{-i\theta/2(\cos(q_x+q_y)\sigma_1 + \sin(q_x+q_y)\sigma_2)} e^{-i\theta(\cos(2q_y)\sigma_1 + \sin(2q_y)\sigma_2)} e^{-i\theta\sigma_1} e^{-i\theta/2(\cos(q_x+q_y)\sigma_1 + \sin(q_x+q_y)\sigma_2)}, \quad (19)$$

where  $\theta = CT/3$  is the coupling angle for a single modulation step.  $\mathcal{U}_{\frac{T}{6}, q_y}(q_x)$  is conveniently symmetric with respect to  $\sigma_3$  for both the parameter values  $q_y = 0$  and  $q_y = \pi/2$ , which implies that the chirality relation 17 between  $A_{q_y}(q_x)$  and  $B_{q_y}(q_x)$  is satisfied with  $\Gamma = \sigma_3$ . When writing the unitary evolution operator for the two symmetry points  $k_y = 0, \pi/2$  we obtain the following forms:

$$\mathcal{U}_{\frac{T}{6}, 0}(q_x) = e^{-i\theta/2(\cos(q_x)\sigma_1 + \sin(q_x)\sigma_2)} e^{-i\theta\sigma_1} e^{-i\theta\sigma_1} e^{-i\theta/2(\cos(q_x)\sigma_1 + \sin(q_x)\sigma_2)} \quad (20)$$

that can be decomposed in  $\mathcal{U}_{\frac{T}{6}, 0}(q_x) = B_0(q_x)A_0(q_x)$ , with

$$A_0(q_x) = \begin{pmatrix} \cos\left(\frac{\theta}{2}\right)\cos(\theta) - e^{iq_x}\sin\left(\frac{\theta}{2}\right)\sin(\theta) & -ie^{-iq_x}\cos(\theta)\sin\left(\frac{\theta}{2}\right) + \cos\left(\frac{\theta}{2}\right)\sin(\theta) \\ -ie^{iq_x}\cos(\theta)\sin\left(\frac{\theta}{2}\right) - \cos\left(\frac{\theta}{2}\right)\sin(\theta) & \cos\left(\frac{\theta}{2}\right)\cos(\theta) - e^{-iq_x}\sin\left(\frac{\theta}{2}\right)\sin(\theta) \end{pmatrix}; \quad (21)$$

and

$$\begin{aligned} \mathcal{U}_{\frac{T}{6}, \frac{\pi}{2}}(q_x) &= e^{-i\theta/2(\cos(q_x)\sigma_2 - \sin(q_x)\sigma_1)} e^{i\theta\sigma_1} e^{-i\theta\sigma_1} e^{-i\theta/2(\cos(q_x)\sigma_2 - \sin(q_x)\sigma_1)} \\ &= e^{-i\theta/2(\cos(q_x)\sigma_2 - \sin(q_x)\sigma_1)} e^{-i\theta/2(\cos(q_x)\sigma_2 - \sin(q_x)\sigma_1)} \end{aligned} \quad (22)$$

That can be decomposed in  $\mathcal{U}_{\frac{T}{6}, \frac{\pi}{2}}(q_x) = B_{\frac{\pi}{2}}(q_x)A_{\frac{\pi}{2}}(q_x)$ , with

$$A_{\frac{\pi}{2}}(q_x) = \begin{pmatrix} \cos\left(\frac{\theta}{2}\right) & -ie^{-iq_x}\sin\left(\frac{\theta}{2}\right) \\ -ie^{iq_x}\sin\left(\frac{\theta}{2}\right) & \cos\left(\frac{\theta}{2}\right) \end{pmatrix} \quad (23)$$

The corresponding  $B_{q_y}(q_x)$  operators can be retrieved from the chirality transformation 17

By evaluating, for the two symmetry points, the winding numbers  $W[f] = \frac{i}{2\pi} \oint_{BZ} dq_x f^{-1} \frac{df}{dq_x}$  of the diagonal and off diagonal terms for  $\theta \in ]\pi/3, 2\pi/3[$  corresponding to the targeted anomalous Floquet topological phase, we obtain the values reported in the first two columns of the following table I. As discussed in the main text, the effect of a diagonal detuning is to rigidly shift the quasi-energy spectrum by a quantity  $\Delta\epsilon = \delta$ . A detuning of  $\delta = \pi/T$  shifts a quasienergy  $\epsilon = 0$  to  $\epsilon = \pi/T$  and *viceversa* therefore the topological invariant for the detuned system can be directly obtained from the tuned one. If the interface between gap-exchanged regions is considered, then the topological index

Gap	in-tune		$\pi/T$ detuned	
	$q_y = 0$	$q_y = \pm\pi/2$	$q_y = 0$	$q_y = \pm\pi/2$
$\epsilon = 0$	0	-1	1	0
$\epsilon = \pm\pi/T$	1	0	0	-1

Table I. Gap winding numbers at high symmetry points of the parametrized 1D model

varies accordingly to table I and the bulk-edge correspondence principle predicts topologically protected 0D interface modes both at the 0 and  $\pi$  gaps in the two symmetry points  $q_y = 0$  and  $q_y = \frac{\pi}{2}$ .

We here note that 0D states emerging on the same bandgap (i.e. 0-gap states at  $q_y = 0, \pm\pi/2$ ) have the same chirality, defined as the sign of the winding number difference between the left and right subsystem, which is opposite to the chirality of the states emerging on the other bandgap (i.e.  $\pi$ -gap states at  $q_y = 0, \pm\pi/2$ ). This difference between the 4 emerging 0D topologically protected states might be related to how they connect to each other forming TET states for  $q_y \in ]0, \pm\pi/2[$ . In particular this might explain why such connection does not cross the bulk bands which would give rise to topological 1D states.

- 
- [1] T. Morimoto, H. C. Po, A. Vishwanath, Floquet topological phases protected by time glide symmetry, *Phys. Rev. B* **95**, 195155 (2017).  
[2] K. Mochizuki, T. Bessho, M. Sato, H. Obuse, Topological quantum walk with discrete time-glide symmetry, *Phys. Rev. B* **102**, 035418 (2020).